
APPENDIX H:
ACOUSTIC CALIBRATION AND MODELING OF SEISMIC SOURCES ON
THE RV *LANGSETH* (2007-2008)



R/V *Marcus G. Langseth* seismic source: Modeling and calibration

John B. Diebold, Maya Tolstoy, Lindsey Doermann, Scott L. Nooner, Spahr C. Webb, and Timothy J. Crone

Lamont-Doherty Earth Observatory, Earth Institute at Columbia University, 61 Route 9W, Palisades, New York 10964, USA (tolstoy@ldeo.columbia.edu)

[1] This paper presents analyses of calibration data of the R/V *Marcus G. Langseth* seismic sources that were collected in 2007–2008. The analysis includes measurements of the levels and azimuthal directivity of the *Langseth* two-string source, which is used for 3-D seismic surveys and compares these data with multichannel seismic hydrophone array data in shallow water. The analysis also shows the important contribution of seafloor and subseafloor reflected and refracted arrivals and the associated effects of water depth and seafloor slope. As expected and predicted by modeling, azimuthal directivity depends greatly on the “footprint” dimensions of the seismic array. In shallow water, where the acoustic field is dominated by near-vertically traveling reflected and refracted waves, data recorded using a towed MCS array are a useful proxy for single hydrophone calibration data. In deeper water, the easily modeled direct arrivals are exceeded in amplitude by seafloor reflected and subseafloor refracted energy at offsets which depend upon the water depth, limiting the applicability of a priori modeling that does not include these interactions. In addition, in a seafloor sloping environment, amplitudes depend greatly on whether the receivers are up-slope or downslope from the source.

Components: 6000 words, 18 figures.

Keywords: seismic source; calibration; modeling; marine mammals.

Index Terms: 3025 Marine Geology and Geophysics: Marine seismics (0935, 7294); 0902 Exploration Geophysics: Computational methods: seismic; 0550 Computational Geophysics: Model verification and validation.

Received 7 May 2010; **Revised** 25 October 2010; **Accepted** 3 November 2010; **Published** 29 December 2010.

Diebold, J. B., M. Tolstoy, L. Doermann, S. L. Nooner, S. C. Webb, and T. J. Crone (2010), R/V *Marcus G. Langseth* seismic source: Modeling and calibration, *Geochem. Geophys. Geosyst.*, 11, Q12012, doi:10.1029/2010GC003216.

1. Introduction

[2] Calibration of the “standard” R/V *Langseth* seismic source arrays was carried out in the NW gulf of Mexico during late 2007 and early 2008 (Figure 1). Initial calibration results for the *Langseth* four-string source array that is typically used for 2-D seismic reflection and refraction surveys were presented by Tolstoy *et al.* [2009] for the two end-member environments (shallow and deep water) chosen for the calibration effort. Here we present

work that includes further refining of the navigation of the calibration buoy hydrophone at the intermediate/slope and deep water sites, as well as analysis of the two-string array results, including its directivity and effects due to subseafloor interaction of sound waves at those sites. The two-string array is typically used for 3-D seismic reflection in a flip-flop mode where four strings are deployed, but only two strings are fired per source point.

[3] One of the fundamental motivations for the *Langseth* calibration efforts was the need to assess

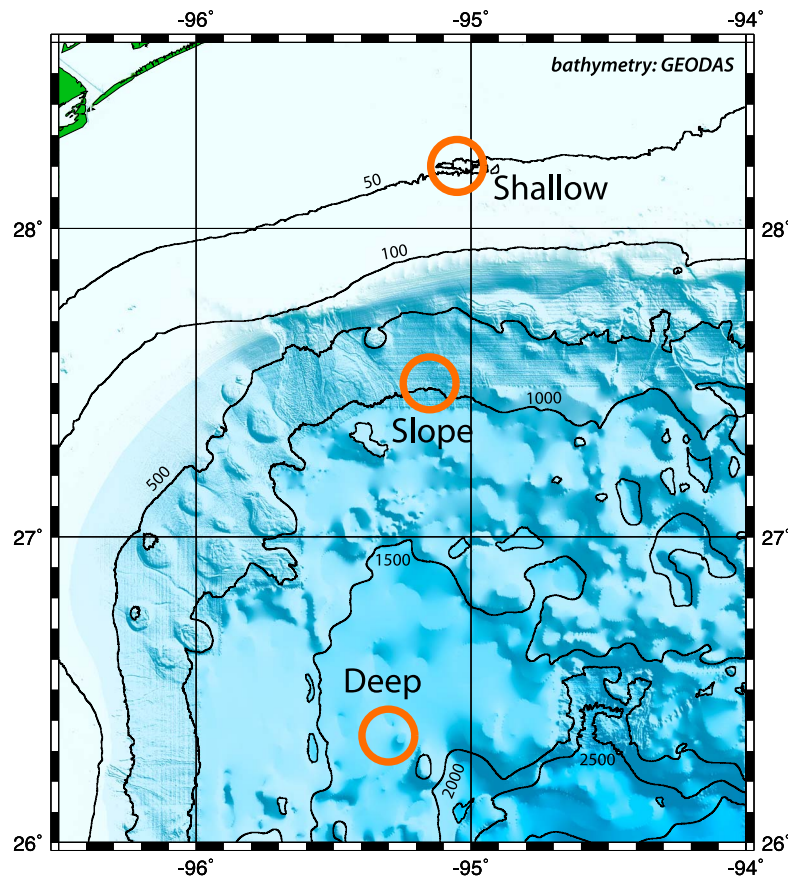


Figure 1. Location map for the three calibration sites, superimposed upon GEODAS bathymetry. Contours are labeled in meters. The shallow site was occupied during cruises MGL0707 and MGL0802; the slope and deep sites were occupied only during MGL0802.

and verify the accuracy and applicability of modeling which has been used to estimate sound pressure levels (SPL) for adherence to marine mammal mitigation guidelines. The amount of time available for the calibration work limited the number of parameters and configurations that could be tested, especially source towing depth, which in practice may vary between 6 and 18 m. If the modeling can be verified for a few basic configurations, then it can be used to reliably predict the effects of small configuration changes.

[4] Previous results were presented using two metrics: SEL (sound exposure level, which is equivalent to energy flux density) and the 90% RMS values favored in the past for evaluation of behavioral responses of marine mammals to anthropogenic noise. Under certain circumstances, these two measures produce the same result, but for impulsive sources, including air gun arrays, 90% RMS is usually higher. As Madsen [2005] demonstrated, the exact difference is highly variable, depending on impulsivity, which may vary greatly for signals containing similar energy levels. Southall

et al. [2007] have recommended that SEL be used instead, and we follow this practice here.

[5] In this paper we present the direct arrival modeling technique used for a priori SPL prediction, and then discuss calibration measurements from the shallow, deep and slope sites and compare. Our goal is to provide calibration results useful for mitigation purposes during *Langseth* operations, and to illustrate how modeling and in situ work can help refine these results for specific sites of operation. We also provide an overview of different factors that should be considered with respect to water depth and source configuration when planning mitigation efforts.

2. Direct Arrival Modeling for Mitigation

[6] A simple ray trace-based modeling approach, assuming an isovelocity sound speed profile, has been used to establish a priori safety radii for marine mammal mitigation during *Langseth* expeditions,

and, previously, for R/V *Ewing*. One of the many motivating factors for the *Langseth* calibration efforts was to assess the accuracy of that modeling. Briefly, the modeling process is this:

[7] 1. Define the air gun array in terms of the size and relative location of each air gun [X, Y, Z].

[8] 2. Model the near field signatures using PGS Nucleus's MASOMO (Marine Source Modeling) and extract them (<http://www.pgs.com/upload/Nucleus.pdf>).

[9] 3. Decide upon a 2-D mesh of points, for example within a plane intersecting the center of the air gun array. Coarse meshes produce smoother contours, but may not fully represent the pressure field, especially near the free surface. A typical mesh is 100×50 .

[10] 4. For each of the points in the mesh, create the signal that would be observed there when every air gun in the array was fired simultaneously.

[11] 5. For that signal, determine the desired statistic: Peak-to-peak dB, Peak dB, RMS dB, maximum psi, etc.

[12] 6. Contour the mesh.

[13] 7. Determine radii and the trajectory of maximum SPL from contour lines (Figure 2).

[14] Most of the work lies in step 4, which has steps of its own:

[15] 1. For each of the air guns in the array, determine the distances, and thus the time of flight between the air gun and the mesh point, as well as the free surface ghost "image" of the air gun and the mesh point.

[16] 2. Scale and shift the air gun near field signal, dividing by the point-to-point distance and moving forward in time according to time of flight.

[17] 3. Scale and shift the near field signal's ghost image, as above, in addition multiplying by the free surface reflection coefficient (typically between -0.9 and -0.95).

[18] 4. Sum the results. For the *Langseth* 36-air gun array, that requires combining the 72 scaled and shifted direct and ghost signals at each mesh point.

[19] These steps are all carried out in the time domain, necessitating resampling. With fine meshes, some numerical jitter is introduced (Figures 2 and 3).

[20] As illustrated in Figure 2, sound levels recorded by the calibration hydrophones will not always be the maximum values, which should be

used for mitigation. Nonetheless, the modeling can be easily adapted to compare it directly with the calibration results (Figure 3). Modeled data points can be calculated and plotted along any desired line (Figure 3) or plane (Figures 2 and 4). Choosing a horizontal plane, as in the case of Figure 4, produces an image of an array's azimuthal directivity.

3. Experiment Design

[21] The calibration field program was conducted over two short cruises (MGL0707 and MGL0802) with the goal of calibrating the R/V *Marcus Langseth* seismic sources, and comparing them with calibration of the R/V *Maurice Ewing* seismic sources conducted in the Gulf of Mexico in 2003 [Tolstoy *et al.*, 2004]. The 2003 measurements were carried out in an area of strong gyre activity, so the *Langseth* effort was moved westward to try to avoid the fast and curved drifting of the unanchored buoy observed away from the shallow sites for the *Ewing* calibration.

[22] Details of the air gun array and the spar buoy used to record it are provided by Tolstoy *et al.* [2009]. The receiver, a spar buoy with two hydrophone channels, was moored at the shallow site (Figure 1) and floated freely at the deeper sites. Detected signals were recorded internally at the buoy, whose position was periodically relayed to *Langseth* by radio. Two issues complicate our analysis. First, a continuous series of low-level noise bursts was superimposed on the recorded calibration buoy data, resulting from the regular radio transmissions of its GPS position. Second, due to the fact that the calibration legs were carried out concurrently with the initial setup and testing of *Langseth*'s seismic equipment, that was not yet complete, the relative positioning of the multistring air gun array, normally provided by GPS signals from modules located within each subarray, or "string" was not yet available. As a result of this, changes in the overall width of the multistring source arrays, expected to occur during turns, could not be verified. Due to the resulting uncertainty, data acquired during tight turns was excluded from the analysis in some cases.

4. Shallow Site: Two-String Array and Its Directivity

[23] Analysis of the four-string *Langseth* source calibration measurements at the shallow site was presented by Tolstoy *et al.* [2009]. Similar analyses for the two-string array measurements are pre-

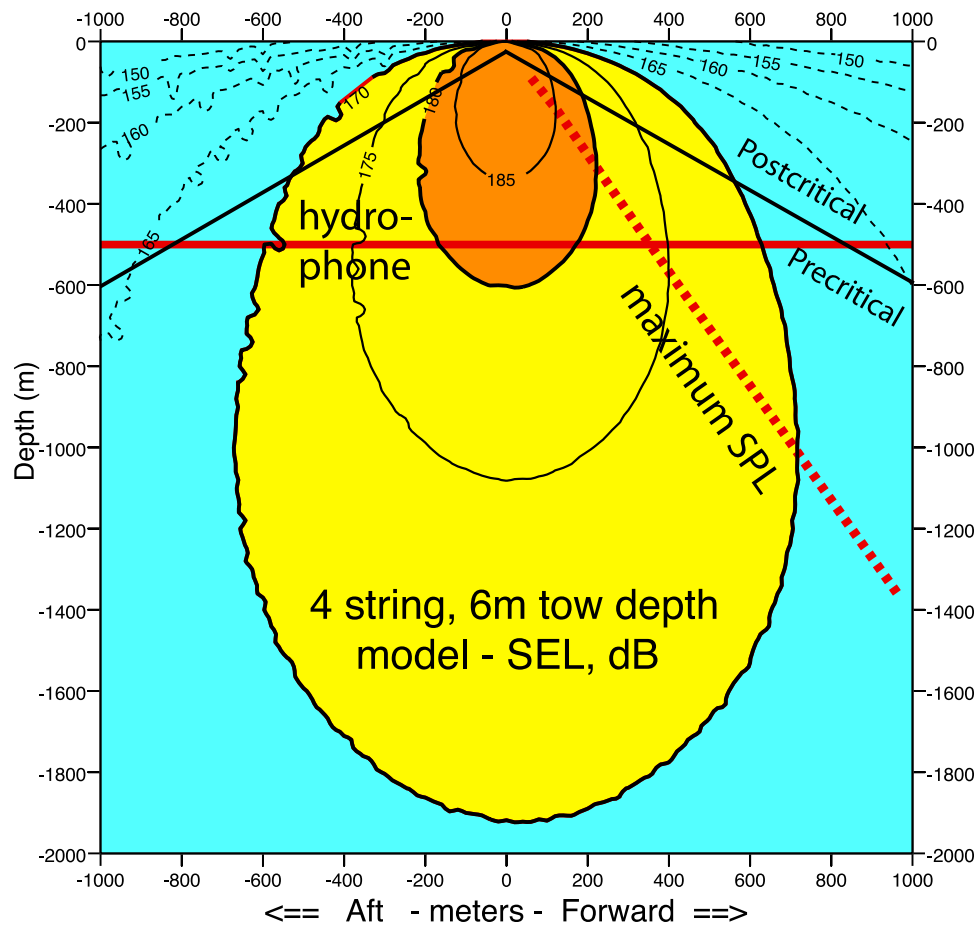


Figure 2. The direct arrival model relevant for deep water for *Langseth*'s four-string air gun array, towed at 6 m depth, the configuration used during the calibration procedure. While the calibration results should be compared to values modeled along the constant depth “hydrophone” line, the maximum values, used for mitigation radii, are found along the slanted, dashed line. Energy which would be postcritically (i.e., totally) reflected or refracted at or below the seafloor propagates from the source and the sea surface in the field labeled “postcritical.” The angle of the dividing line separating precritical and postcritical depends on the velocity of sound below the seafloor, and the x value of the point at which this line intersects the seafloor is called the “critical distance.”

sented here. The two-string array is essentially a subset of the four-string array, comprising two of the four identical nine-element linear subarrays with the same 8 m string-to-string separation used in the four-string array. The two-string array is thus aurally 1/3 as wide as the four-string array, while having the same length. Thus its predicted azimuthal directivity is considerably different (Figure 4). Like an antenna, the directivity of a source array is highly dependent upon its dimensions. The larger the dimension of the array in any particular direction, the smaller and more tightly focused its beam pattern in the same direction. Since the *Langseth* two-string and four-string arrays have the same along-track dimensions, the difference in their inline power is controlled only by the number of air guns in the respective arrays, two to one, equating to a 6 dB difference. In the cross-line or athwart-

ships direction, however, the difference in physical extent tends to counteract the difference in number of elements, and received energy levels are nearly the same for both arrays.

[24] As described by *Tolstoy et al.* [2009] the shallow site shooting pattern was designed to maximize the number of impulses recorded in the orthogonal fore and aft (inline) and athwartships (cross-line) directions. Measurements of the two-string array were made twice at the shallow site, and thus this site provides the best coverage, especially in the cross-line direction. Figure 5a shows the sound exposure level (SEL) for the cross-line direction and Figure 5b shows the SEL for the inline shots. In the inline direction, the measured two-string array levels are about half (6 dB) those of the four-string array. In the athwartship, or cross-

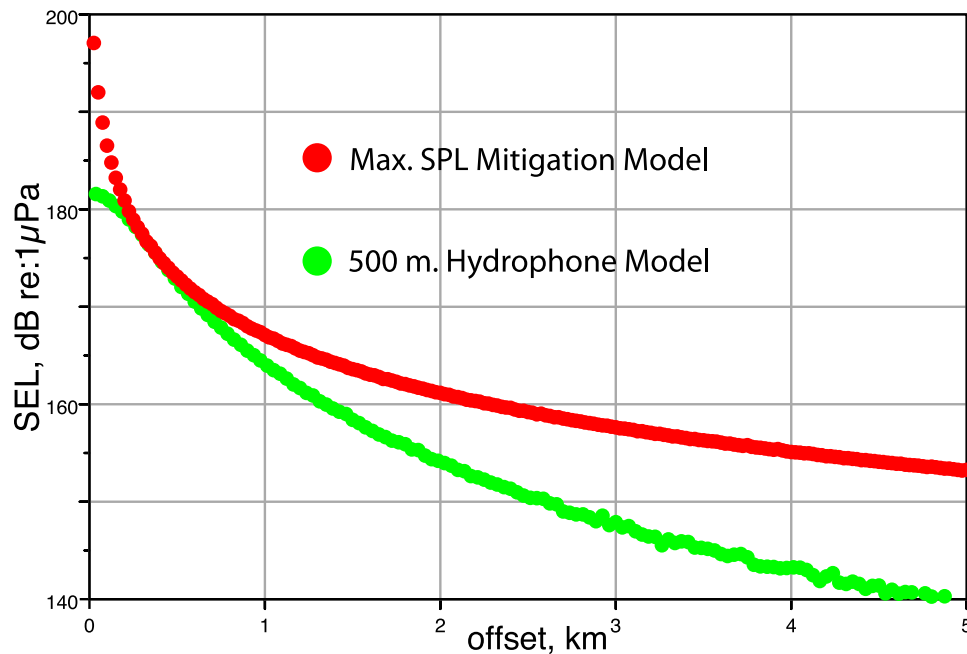


Figure 3. The modeled sound exposure levels along the hydrophone depth and maximum SPL lines drawn in Figure 2. The green line should be compared to the calibration results, while the red line is used to establish mitigation radii.

line direction, the measured levels are about 5 dB higher, thus almost equivalent to those of the four-string array. For comparison with the root-mean-square (RMS) method of calculating received levels RMS and SEL values for all shallow site shots are shown in Figure 5c.

[25] In general, exposure levels produced by the two-string array are nearly twice as high (5 dB) to the side as they are inline. In addition, there is a pronounced increase in local variation in the athwartships levels. This variation appears to be due to topography, rather than array effects. This explanation is based upon the high level of similarity in the variations in two physically coincident data sets, where data from the four-string and two-string arrays can be directly compared. The conclusion that amplitude variations in the athwartships direction are controlled by subtle changes in topography is supported by a comparison of parts of the MGL0707 four-string and MGL0802 two-string calibration data that were shot along a physically coincident part of the spiral track (Figure 7).

[26] Criteria for the shallow site were that it be free of obstructions, removed from ship traffic, and relatively flat. The chosen 35×22 km area met those conditions, and the spiral pattern was aligned with the long, inline segment along strike, as determined from preexisting bathymetric charts. Echo sounder records from MGL0707 (Figure 6a)

show that in fact, the seafloor dips gently along this line, and is about 5 m deeper at the WSW end than it is 35 km to the ENE (Figure 6b). More variation (15 m) is seen in the dip direction, covered by the spiral pattern, which spans 22 km (Figure 6b). Although these latter variations are slight, they do affect the data.

[27] The most profound amplitude variations are the deep and sharply notched lows observed along the spiral track at source-receiver offsets of 11 km, 12.4 km and 14 km (Figure 7). Flanking (possibly) high values are more smoothly spread out. There is no complete high-resolution bathymetry map of the area, but it is likely that the sharp, low values are due to topographic shadowing or defocusing. The observation that these low values are present for both source arrays leads to the conclusion that they do not result from the directivity of the two-string array.

[28] Another remarkable amplitude anomaly is the abrupt increase at source-receiver offsets of 800 m in the inline direction (Figure 5b). A likely explanation, borne out by previous observation and modeling [Diebold *et al.*, 2006] is that the lower, near-offset trend corresponds to direct arrivals; those with the minimum source-receiver path, and that the higher, larger-offset trend corresponds to postcritically refracted and water-borne multiply reflected arrivals. This interpretation is supported by the multichannel seismic (MCS) data collected

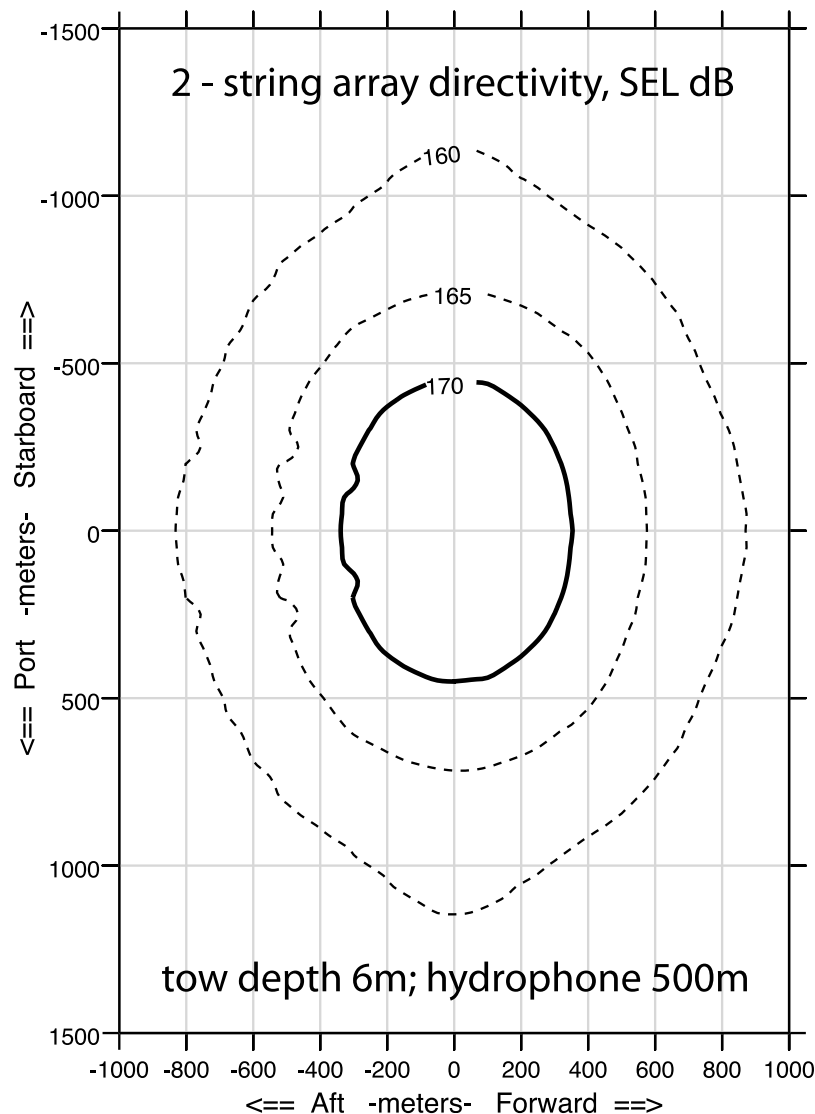


Figure 4. Modeled aerial directivity for the *Langseth* two-string seismic source with the same 6 m tow depth that was used in the calibrations, as observed at 500 m below the sea surface. 500 m was the intended hydrophone depth used at the intermediate and deep calibration sites. (In practice, depths to the hydrophone range between 350 and 500 m [see Tolstoy *et al.*, 2009].) Predicted sound exposure levels are distinctly higher in the athwartships (“cross-line”) direction than fore and aft (“inline”).

along the inline track during MGL0802 using the two-string source and a 5850 m long hydrophone array. Each of this array’s 468 channels comprised 14 individual hydrophones spread out over 17.75 m with a nominal group spacing of 12.5 m (4 hydrophones at the extremity of each group are shared with the adjacent group). As a result, direct, horizontally traveling arrivals are attenuated, while near-vertically traveling reflected and refracted energy is enhanced. Figure 8a shows an MCS shot gather along the inline track with the two-string source coincident with position previously occupied by the calibration buoy. It can thus be compared

directly with buoy results without concern for subtle bathymetric variations. The comparison is shown in Figure 8b. It is clear that the sound exposure levels derived from the towed hydrophone array data are very similar to the calibration hydrophone data.

[29] Since acoustic propagation in shallow water environments may vary greatly with bottom type and topography [cf. Barton *et al.*, 2006] it seems logical and advantageous that MCS data should be monitored in real time to fine tune a priori mitigation radii in shallow water (100 m and less) environments. These data demonstrate that MCS

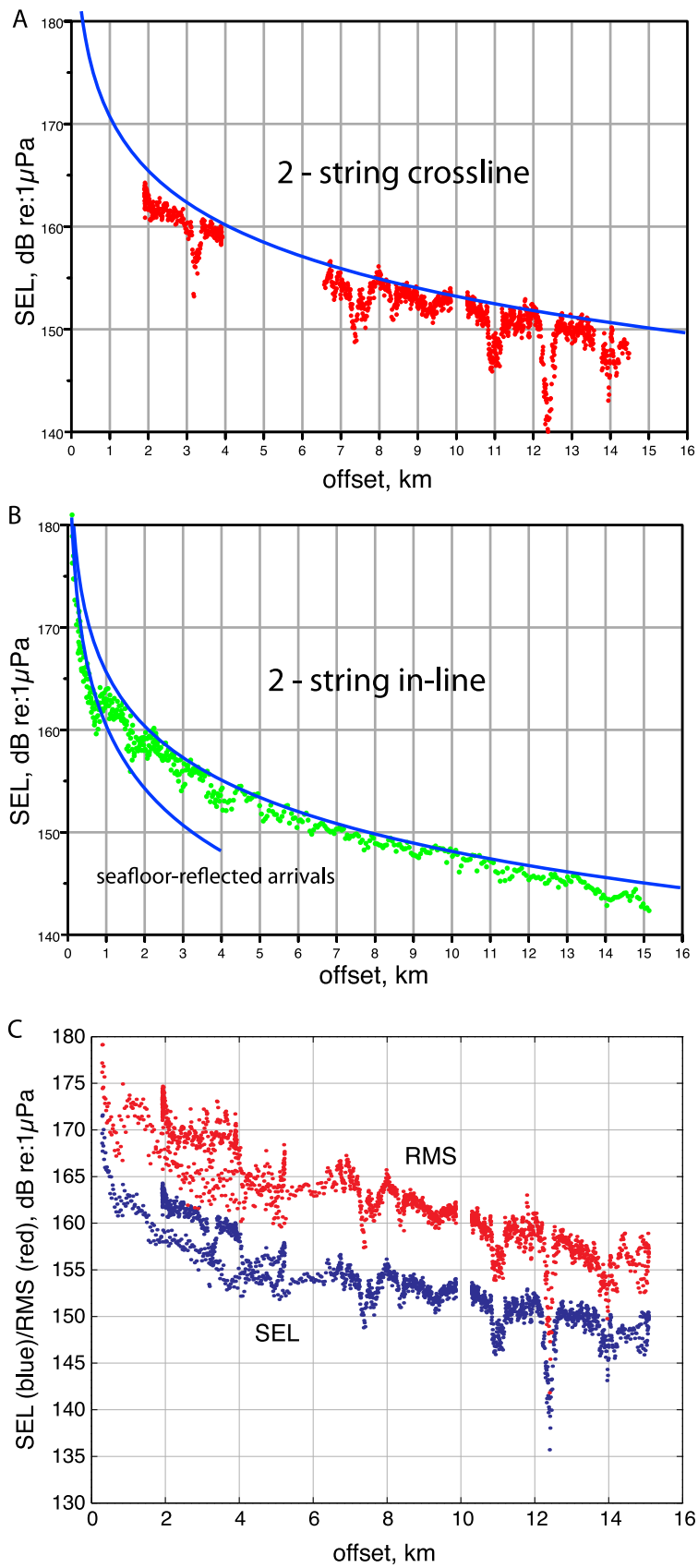


Figure 5

(streamer) data can provide an accurate assessment of SEL levels at the relevant ranges for mitigation in shallow water environments.

5. Deep Site: Two-String Array and Bottom Interaction

[30] Results for the four-string deep site direct arrivals were presented by *Tolstoy et al.* [2009]. In Figure 9a we show the direct arrivals at this site for the two-string array. Inline arrivals are green, and cross-line arrivals are magenta. The directivity seen at the shallow site is still present, with about the same ~ 5 dB difference observed at the shallow site, where cross-line coverage is more complete. Modeled levels for the inline and cross-line directions are also shown. It is apparent that in one case (1.2 km) the measured levels slightly exceed the model. For comparison with the root-mean-square (RMS) method of calculating received levels RMS and SEL values for all shallow site shots are shown in Figure 9b. These data were shot during a small-radius circular turn (Figure 10) and the increase is almost certainly due to the natural tendency of the two towed, linear subarrays to crowd closer together, reducing the separation from the intended 8 m, and thus changing the directivity of the array. The *Langseth* source subarrays are normally equipped with individual GPS units, whose readings can determine the string-to-string spacing, but these were not completely operational during the early stage of operations during which the calibration was carried out. It should also be noted that this kind of sharp turning is not included as part of normal seismic surveys, and data from such turns has not been included in most of the results presented henceforth.

[31] For data recorded at the deep and slope sites, it was possible to separate the direct arrivals from later arrivals, which were reflected from the seafloor or postcritically reflected from (or refracted within) underlying layers. *Tolstoy et al.* [2009] presented only the direct arrival data at the deep site. While at the shallow site the observed wavefield is completely dominated by later arrivals (Figure 8a) at the deep water site the amplitudes of the seafloor arrivals outweigh those of the direct arrivals only

beyond 2.5 km (Figure 11). Amplitudes of these arrivals fall off more or less linearly with increasing offset, except for the increase at about 5.2 km, which almost certainly corresponds to the critical point of the reflected/refracted arrivals. The source-receiver offset at which this critical point is observed depends on water depth and on the velocity of sound in the reflecting layer. The average water depth is 1540 m. The reflection velocity for a 5.2 km critical distance at this water depth is about 1.75 km/s. At the shallow site, the water depth is 50 m and the critical point, as observed in Figures 8a and 8b, is seen at a little less than 1 km offset. This reflected and refracted energy travels at incidence angles closer to vertical than the direct arrivals, and observed amplitudes are much less sensitive to hydrophone depth than those for the direct arrivals. It is thus meaningful to compare these reflected and refracted arrival amplitudes to the maximum amplitude mitigation model results, as is done in Figure 11.

[32] In Figure 12, we present the analogous plot for the four-string source array at the deep calibration site. Again, the critical distance is about 5 km, and the postcritically reflected and refracted arrival amplitudes fall below the mitigation model. It is also clear that the local amplitude structure of the precritical reflections is quite dependent upon the seafloor topography. The SEL of all of the arrivals again fall below the maximum amplitude mitigation model.

6. Slope Site: Four-String Array, Intermediate Water Depth, and Updip and Downdip Variations

[33] Data from the slope site were not presented by *Tolstoy et al.* [2009]. Only the full, four-string array was tested at this location. The calibration buoy was drifting rapidly during the entire shooting period, and the ship track included many small-radius circular turns. It was apparent that the spread of the four source strings was greatly reduced during these turns (though to an unknown extent) and this required some of the turn data to be eliminated from the analysis. In addition, only shots within 5 km of the buoy hydrophone could be

Figure 5. (a) Sound exposure levels for the cross-line (side aspect) arrivals recorded along the spiral track at the shallow water calibration site, with a 95th percentile fit (using the methods described by *Tolstoy et al.* [2009]). (b) Sound exposure levels and 95th percentile fits for inline shots recorded at the shallow site. There is a clear difference in the trend between zero and 0.8 km and that beyond 0.8 km. Separate 95th percentile fits are shown for each trend. (c) Sound exposure levels (blue) versus root-mean-square (red) values for all shallow water shots illustrating the ~ 8 –10 dB offset between the two methods of calculating acoustic received levels.

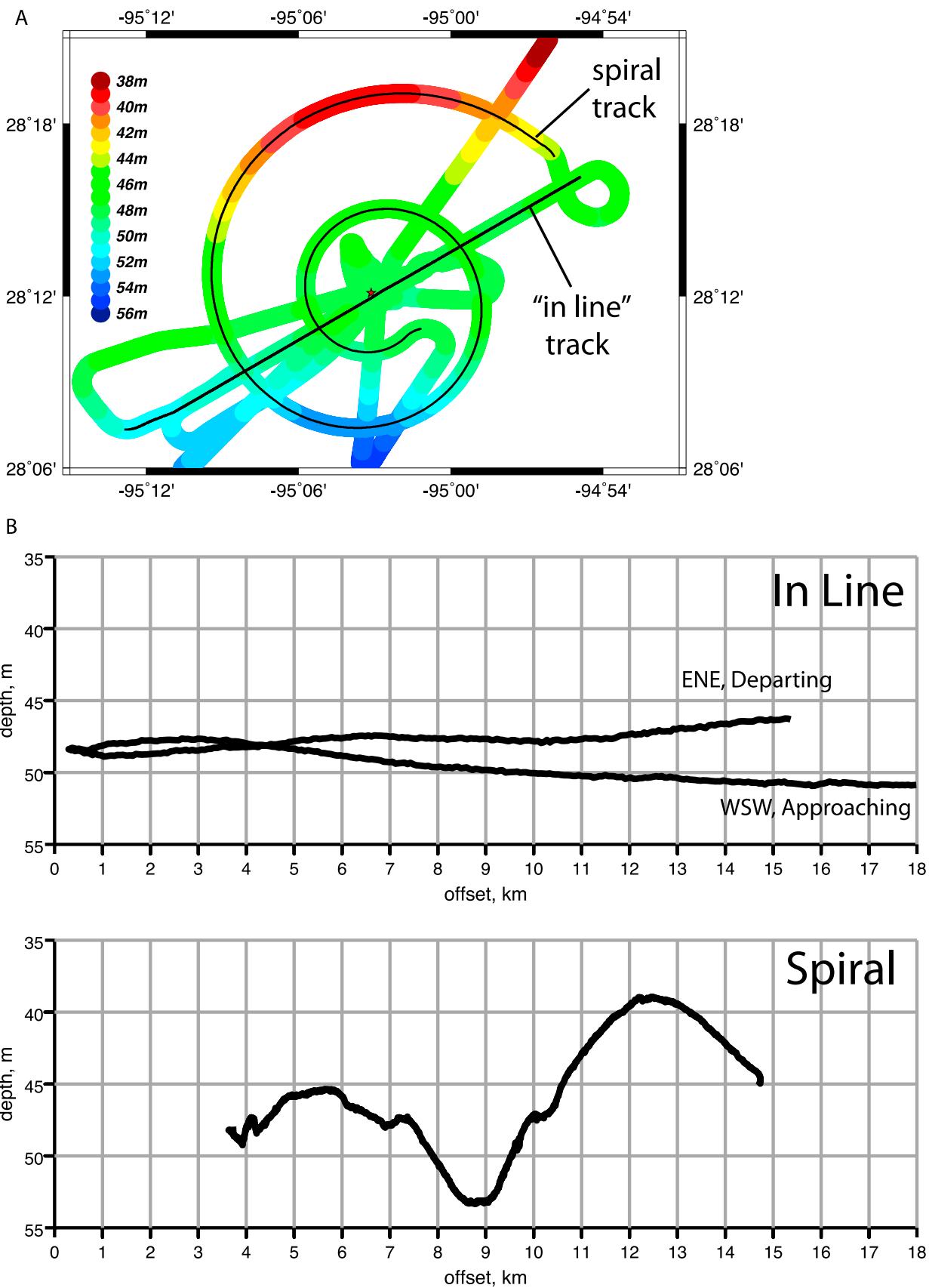


Figure 6

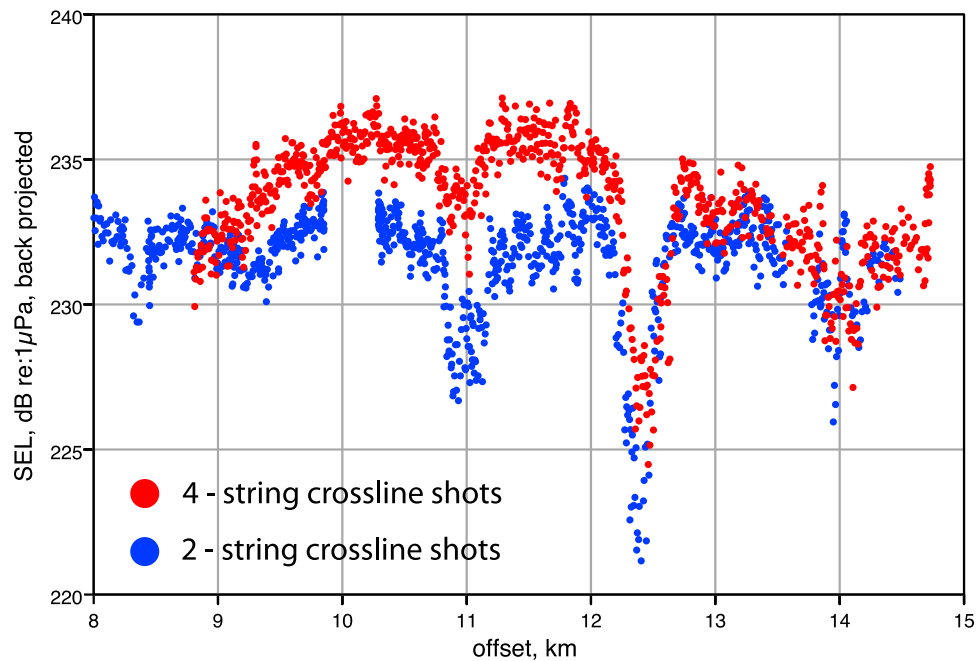


Figure 7. MGL0707 four-string and MGL0802 two-string cross-line source levels recorded along coincident portions of the spiral track (Figure 6a) show strong similarities, particularly in the sharply low levels at 11, 12.4, and 14 km. Offsets correspond to those in Figure 6b, and the low values are likely due to shadowing by slightly elevated knolls. To separate amplitude variations due to changes in source-receiver offset from those due to topography, these sound levels have been back projected to a notional distance of 1 m from the source, i.e., multiplied by a factor equal to the source-receiver offset in meters.

used for the compilation of direct arrivals. At greater source-receiver offsets, windowing of the direct arrival tended to fail, as the measured levels lost coherence because the data were obviously dominated by systematic, ambient, and/or previous shot noise. The source points included in the analysis are shown in Figure 13.

[34] The direct arrival amplitudes for this site are very similar to those observed at the deep site for the two-string and four-string arrays. Figure 14 shows these levels, compared to those predicted by modeling. The fit is good, except at near offsets, where the model underpredicts the observed source levels. This situation is the opposite of the observations at the deep site [Tolstoy *et al.*, 2009] where the near-field effects cause a diminution in source levels at close proximity. It is likely that two factors contribute to this. One hypothesis is that the inter-string spacing was smaller than intended during

these close approaches, but due to the lack of complete GPS positioning on the array strings, this cannot be verified. Second, the sound velocity profile changed considerably between acquisition of the deep and slope site data. An intervening storm increased the thickness of the mixed layer, reduced its velocity, and strongly altered the shape of the thermocline (Figure 15). As in the two previously presented cases (Figures 9 and 12) measured levels fall well below the mitigation model predictions at offsets greater than 2.5 km, due to the downward focusing sound velocity profile.

[35] In Figure 16, energy levels for seafloor-reflected and subseafloor-refracted arrivals are superimposed on the direct arrival levels. At this intermediate-depth site, the crossover is located at 2 km offset, compared to 2.5 km at the deep site. An increase in amplitude, corresponding to the critical distance, beyond which postcritically reflected and refracted

Figure 6. (a) Water depths along the MGL0707 shallow site ship track. Spiral and inline tracks were also occupied during MGL0802. The location of the calibration buoy for both legs is shown by the red solid star. Depths increase modestly from NNW to SSE. (b) Water depths along the inline and spiral tracks of Figure 6a. Along 33 m of inline track, the water depth varies by 5 m. Across 22 km in the orthogonal direction, water depths vary by nearly 15 m. Though small, these differences and local variations in topography affect received sound levels.

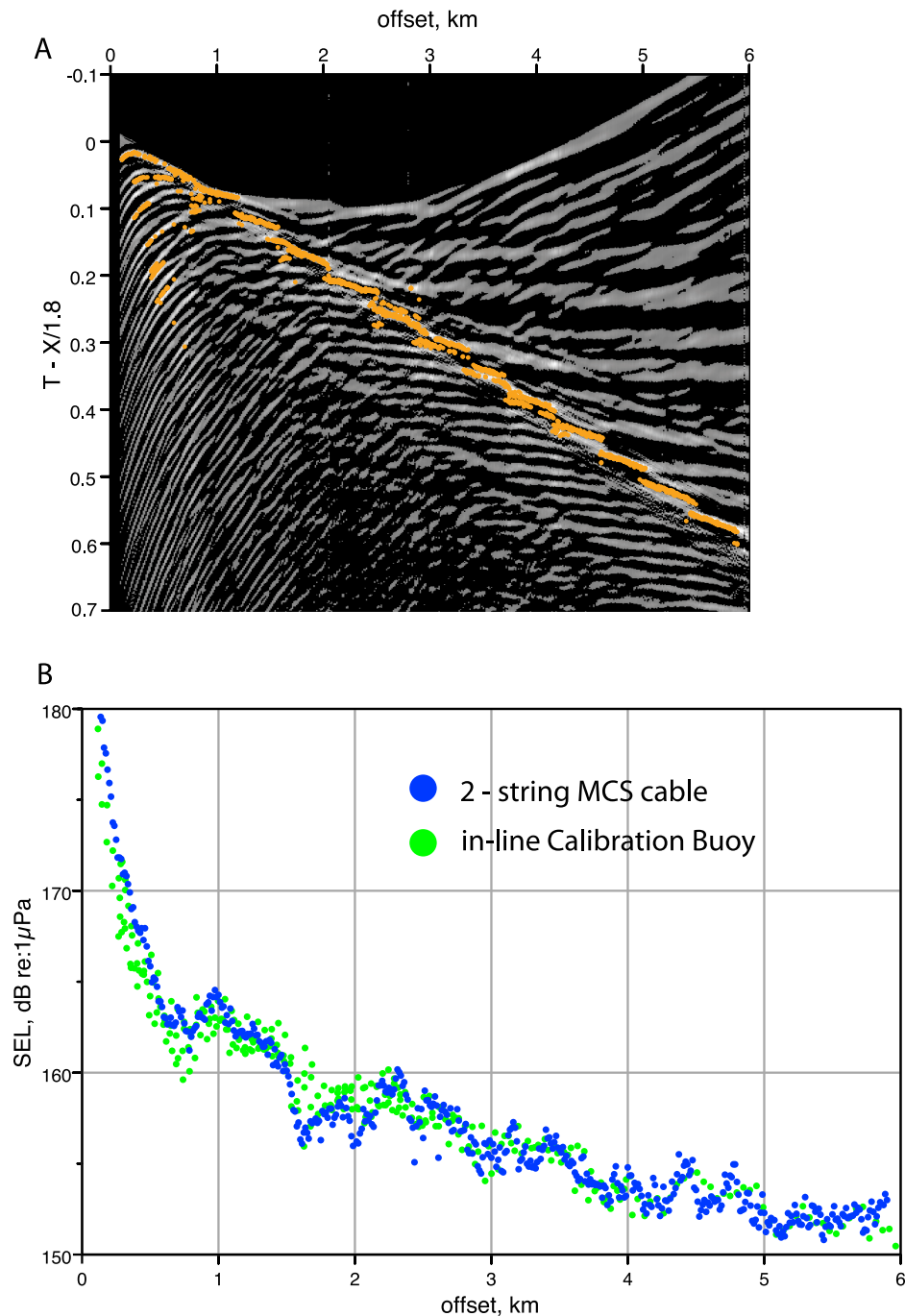


Figure 8. (a) An MCS shot gather along the inline track, with the two-string source coincident with the position previously occupied by the calibration buoy. The peak level for each of the 268 traces is shown in orange (positive data amplitudes are in gray, negative amplitudes are in black, and peaks may be negative as well as positive). Between zero and 0.8 km., the peaks are mostly found on the seafloor primary and multiple reflections, while at larger offsets, they are on the primary and multiple postcritical reflections from deeper layers. (b) SEL, as derived from the MCS shot gather of Figure 8a, compared to the two-string inline calibration buoy data, acquired along the same track.

arrivals are generated, is seen at about 4 km (as compared to 5 km for the deep site). The singular excursion observed as peaking at 2.9 km is certainly due to seafloor topography, though the exact cause was not determined. There is a notable bifurcation

of levels for the bottom-interacting arrivals at source-receiver offsets greater than 5 km.

[36] It is clear in Figure 16 that the reflected and refracted arrival amplitudes with source-receiver

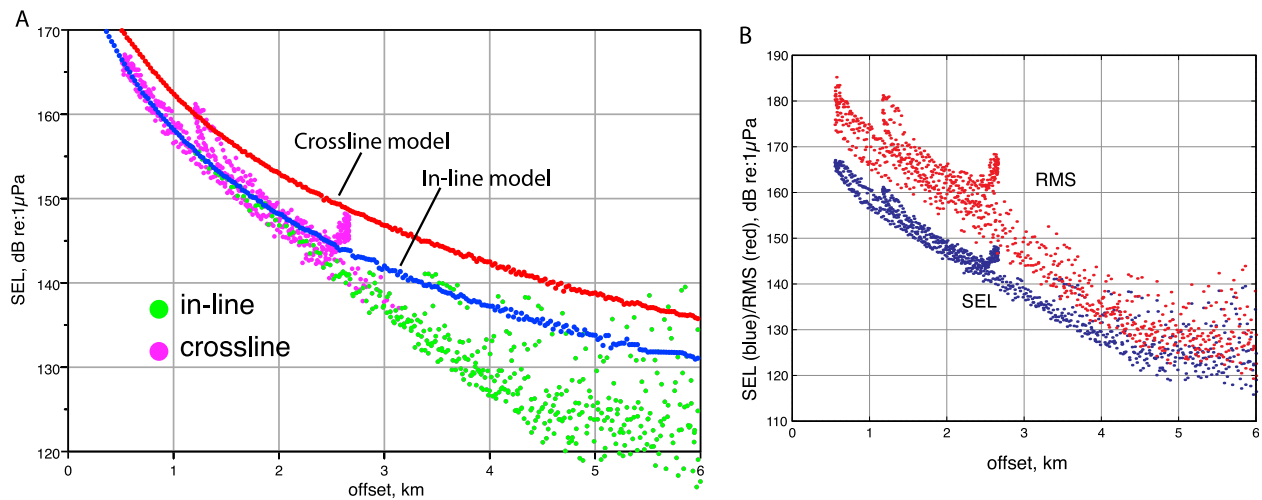


Figure 9. (a) Direct arrivals from the *Langseth* two-string source array, recorded at the deep calibration site. Sound exposure levels for shots with an inline aspect (the receiving buoy in front of or behind the array, $\pm 30^\circ$) are colored green, and others (cross-line, or athwartships) are colored magenta. Model results for a 500 m deep hydrophone are shown in red for cross-line geometry and in blue for inline geometry. (b) Sound exposure levels (blue) versus root-mean-square (red) values for all deep water shots. The offset between the two methods of calculating acoustic received levels varies between 10 and 20 dB for close ranges, gradually decreasing with increasing offset to 5–10 dB.

offsets greater than about 5 km fall along two diverging trajectories. When the source and receiver locations where these trajectories are best defined were identified, it was clear that the differences correspond to the source-receiver geometry in relation to the sloping bathymetry at this calibration site. In Figure 17a, the amplitudes for these arrivals are colored red for shots where the calibration buoy was positioned downdip from the source, and blue for the case where the buoy was upslope from the source points. These relationships are shown in Figures 17b and 17c.

[37] Average water depth for the downdip (red) shots was 800 m, compared to 1050 m for the updip (blue) shots. Despite this difference the critical distance for both sets of shots is about the same: 3.5–4 km. The reason for this, and for the differences in amplitude, is the sloping seafloor. When shooting up dip, rays are concentrated toward the source, focusing energy and shortening the critical distance, while the converse is true when shooting downdip [Levin, 1971; Diebold and Stoffa, 1981].

7. Spectral Content With Offset

[38] Figure 18 shows the variation in the energy spectral density with offset for the inline shots for the deep (Figure 18a) and shallow (Figure 18b) sites. Spectra for some individual shots are shown by Tolstoy *et al.* [2009], but this approach allows for a more comprehensive display of the change in

spectral content with increasing distance from the source. The parallel bands in both the vertical and horizontal directions, that are more pronounced in Figure 18b, are due to bursts of electronic noise associated with the GPS receiver on the recording buoy and is not associated with the *Langseth* sound source. Leakage of the broad spectrum periodic noise into the calibration data was associated with common ground between the data logger and the GPS receiver that was largely resolved for the 2008 deployment by optically isolating the signal coming in. Hence the signal is more pronounced in the shallow inline data that was collected during the first calibration leg in 2007, and barely visible in the deep water data that was collected in 2008. Note that for the deep water site (Figure 18a) the hydrophone is at 350–500 m depth, so the true distances to the source are greater than for the shallow site and change with offset due to the slant range. Offsets shown on the plot are based on surface location of the buoy not considering the depth of the hydrophone. Figure 18a illustrates the rapid drop off in energy with distance from the source, particularly at higher frequencies.

8. Conclusions

[39] Single hydrophone source calibration results in shallow water are sufficient to predict radiated sound levels in similar environments. When calibrations are carried out with a single hydrophone in

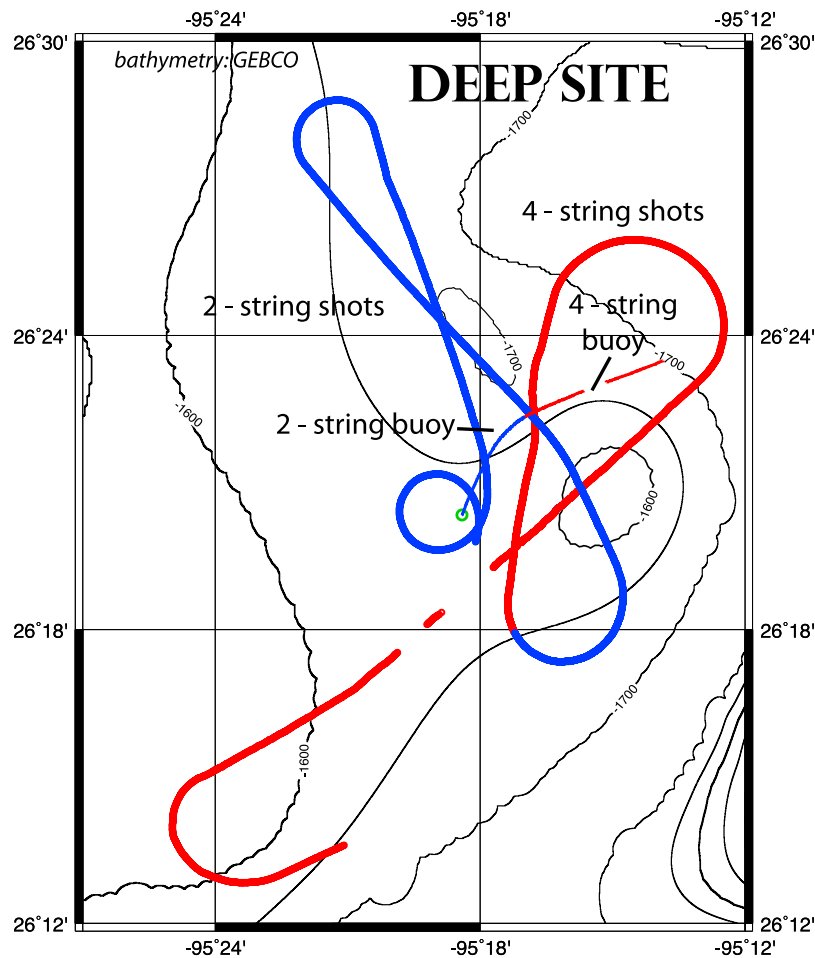


Figure 10. Source and receiver locations for the MGL0802 deep site, with regional depth contours in meters. Two-string locations are shown in blue, and four-string locations are shown in red. The path of the slowly drifting hydrophone buoy is also shown in blue and red.

deeper water, however, the results must be combined with modeling results for extrapolations to full water depths. Our observations and analyses show that the propagation of sound between a marine seismic source comprising an array of air guns and a receiver can be satisfactorily characterized by modeling along direct pathways, though this modeling could be improved by including realistic sound velocity profiles within the water column.

[40] The source array directivity due to the dimensions of the overall footprint of the array, predicted by modeling, is confirmed by a comparison to the results from the R/V *Langseth*'s two-string and four-string array calibrations. Under some conditions (sharp turns, failure of towing equipment) this footprint can be changed, thus altering the array's directivity. Therefore it is essential that the individual source arrays be positioned by differential

GPS antennas and, when appropriate, acoustic transponders. Sharp turns are not normally part of standard seismic operations.

[41] In all water depths, contributions due to acoustic interaction at and below the seafloor are likely to be important as well. These interactions may result from shadowing or focusing due to subtle physical and topographic features, an effect particularly apparent in shallow water and for near-vertically reflected precritical arrivals in deeper water, and are typically difficult to model accurately without a considerable amount of a priori knowledge. In the shallow water environment of our shallow calibration, topographic shadowing effects appear to greatly outweigh focusing effects, if any are indeed present.

[42] Our results indicate that directly propagated arrivals play a small role beyond a few thousand meters range, but that in water depths of 850 m and

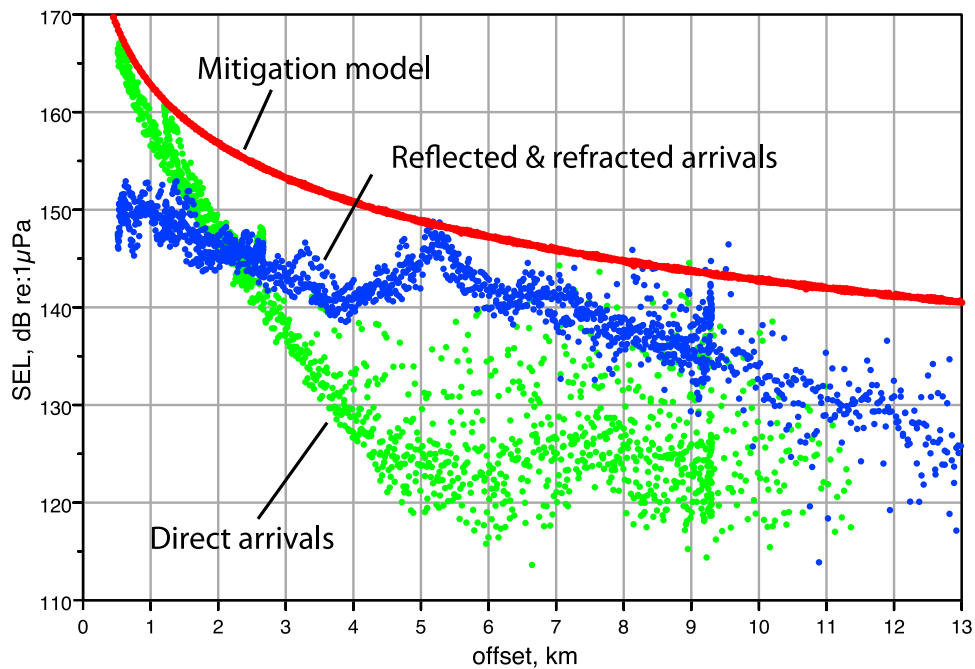


Figure 11. The direct arrival energy flux density (SEL) values of Figure 9a overlap with those of the seafloor and subseafloor reflected and refracted arrivals for the two-string array. These arrivals go postcritical at about 5 km but still fall almost entirely below the maximum amplitude mitigation model. Beyond about 5 km, the direct arrival amplitudes become incoherent, as the data windowing begins to fail and/or instrument and other ambient noise begins to dominate the true arrivals.

more, the seafloor and subseafloor interactions, while present and important, do not exceed safety criteria. Lower sound exposure levels, thought to induce behavioral responses in some animals, will likely be achieved at relatively large distances, but

our results show that in intermediate and deep water depths, the levels observed are not greater than those predicted by the simple modeling currently in use.

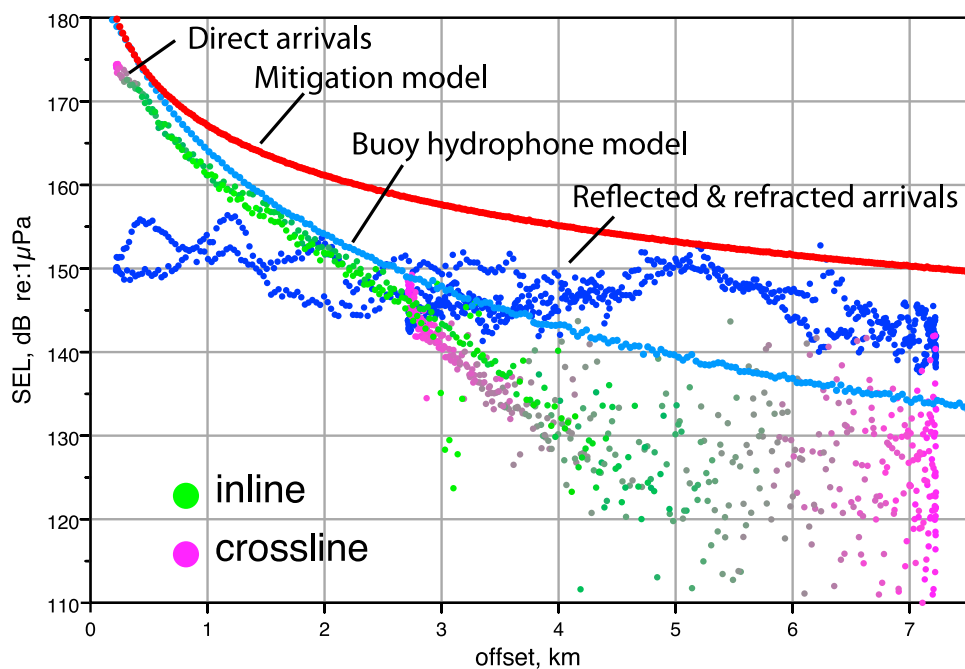


Figure 12. SEL for direct and reflected/refracted arrivals from the four-string array at the deep calibration site.

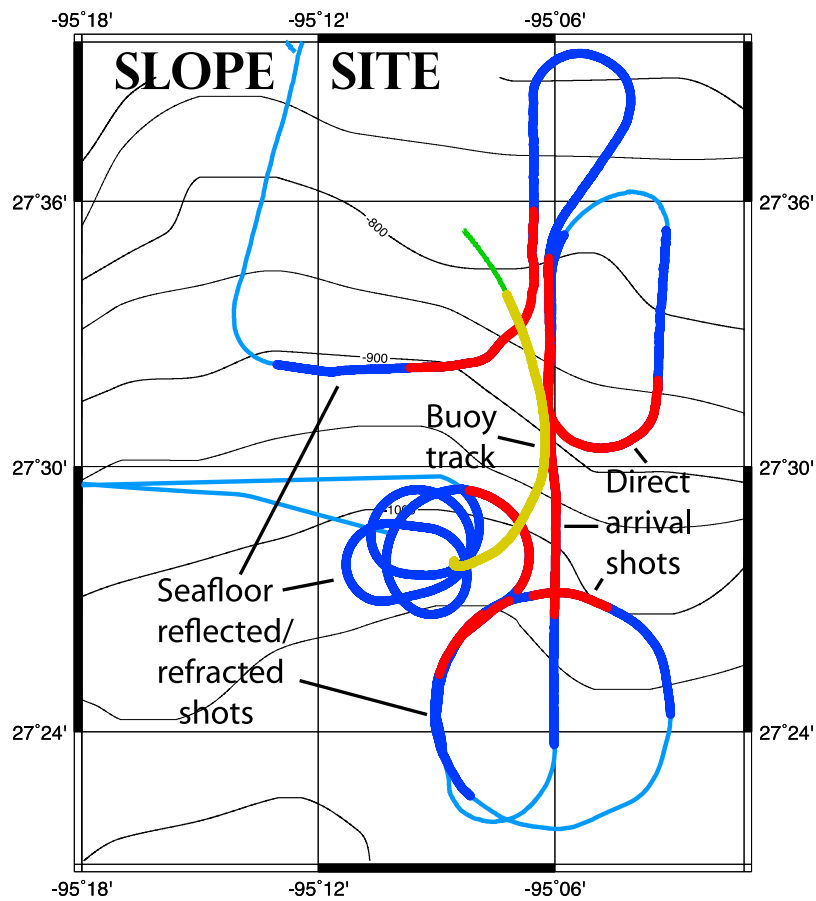


Figure 13. Track map for the slope site calibration. Shots used in the analysis are highlighted in red for those used in the direct arrival compilation and blue for additional shots used in the seafloor and subseafloor compilation. The corresponding buoy locations are mustard colored.

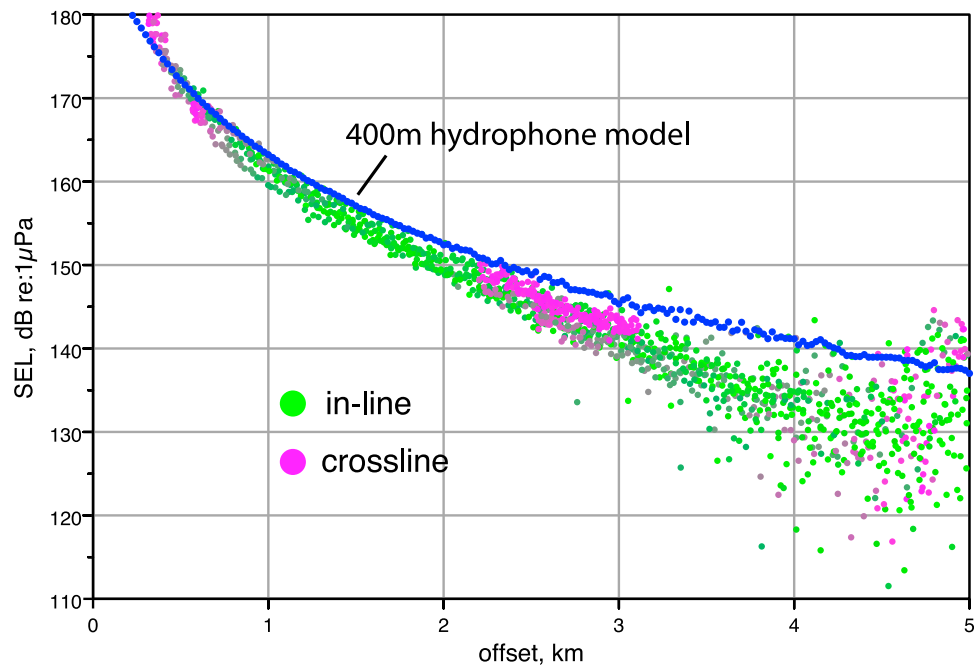


Figure 14. Energy flux density (SEL) values for direct arrivals at the slope site. Inline and cross-line aspects are color coded as before. The four-string model with 6 m tow depth and receiver depth of 400 m is shown for comparison. The model is only exceeded by the data at small offsets.

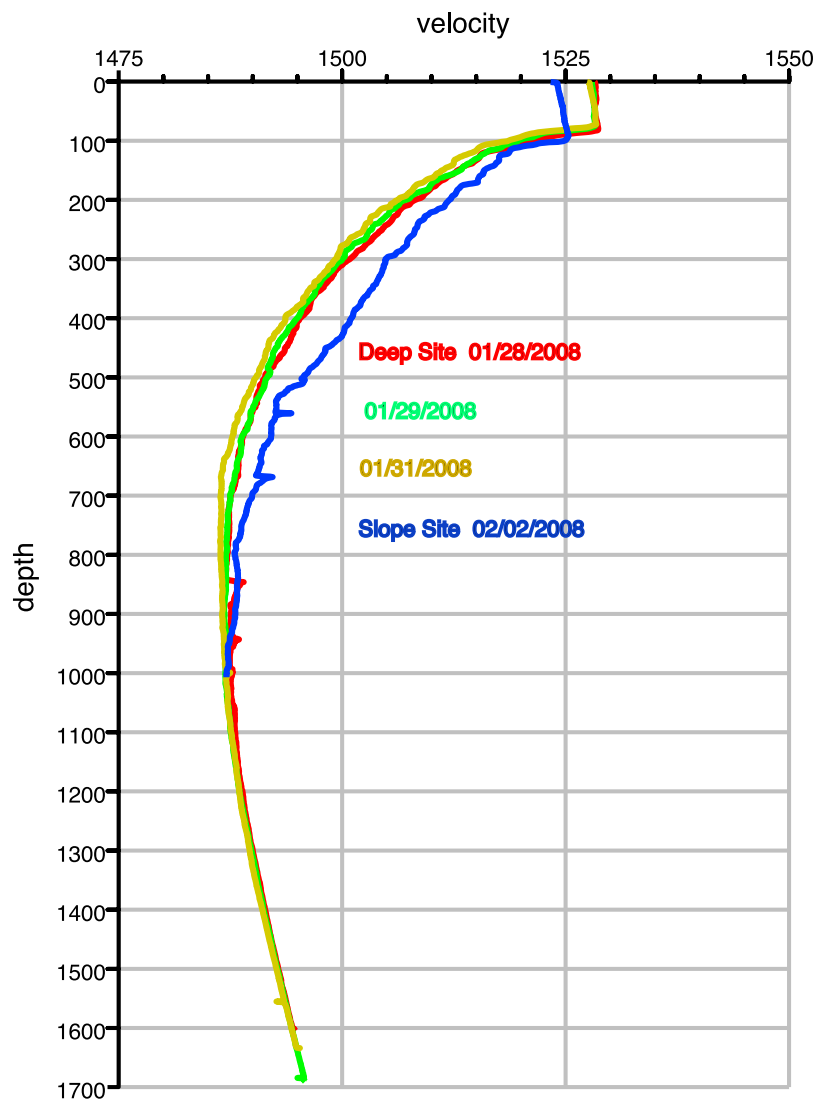


Figure 15. XBT-derived sound velocity profiles covering a span of 6 days during MGL0802. The profiles are very consistent for the first three casts, but a storm on 1 February significantly altered the top part of the profile, after which the slope site data were acquired.

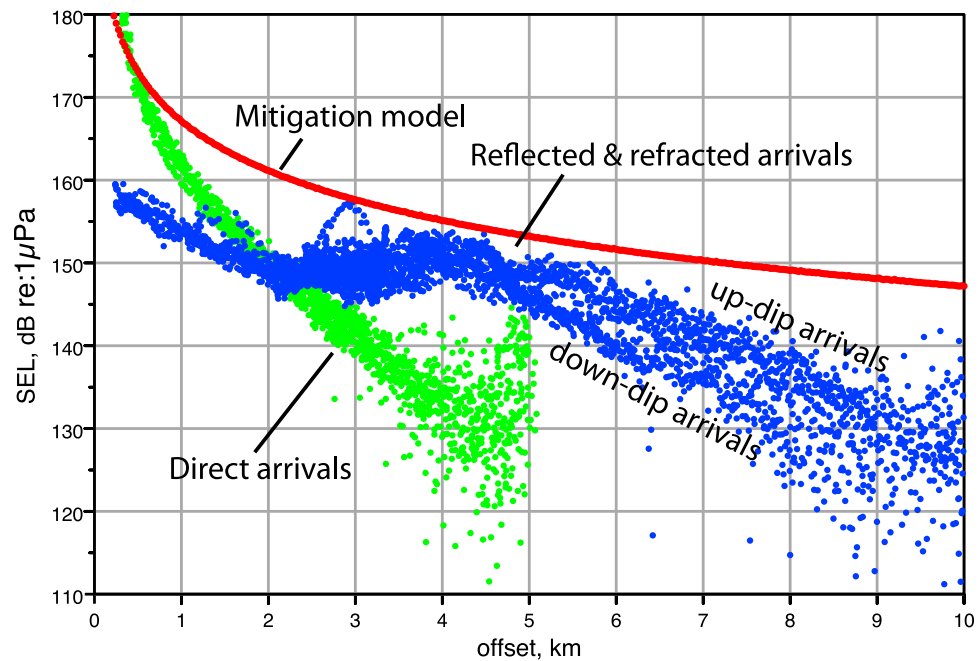


Figure 16. As in Figures 11 and 12, measured levels for seafloor reflected and subseafloor refracted arrivals at the slope site are superimposed on the direct arrival values. Since the water is shallower at this site, the critical distance is 4 km, rather than the 5 km observed at the deep site. All observed levels (except at very near offsets) fall below the mitigation model predictions.

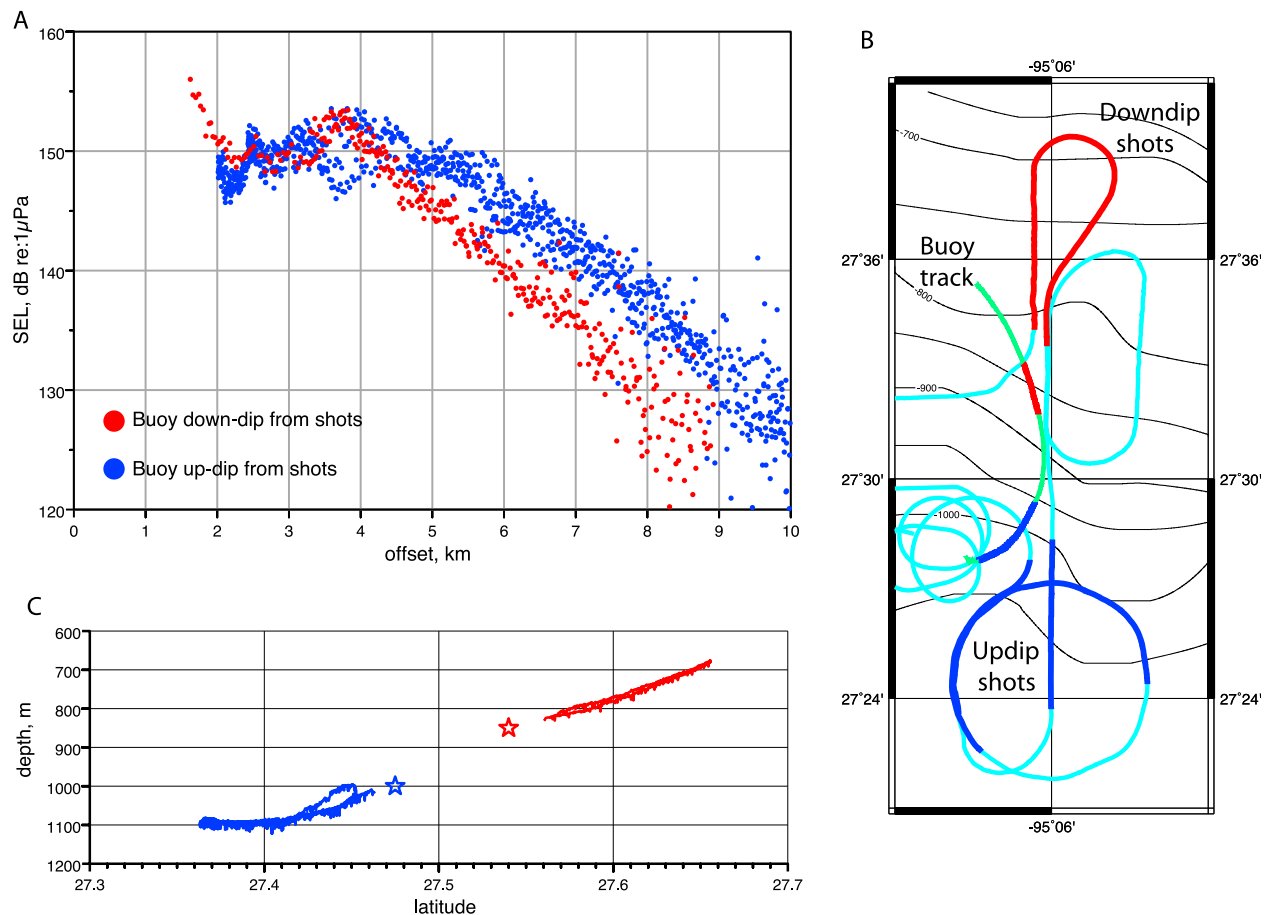


Figure 17. (a) Two subsets of the reflected/refracted arrival levels of Figure 16. Although the critical distances seem similar, there is a clear bifurcation in amplitude falloff at greater offsets (4–10 km). (b) Source and receiver locations for the arrivals of Figure 17a. Color coding (red when the receiver is downdip from the sources and blue for the converse) matches that of Figures 17a and 17c. (c) Seafloor depths beneath the source points used in Figure 17a, projected onto a N–S trending plane. The stars show the latitude and average seafloor depths beneath the calibration buoy hydrophone for the corresponding source points.

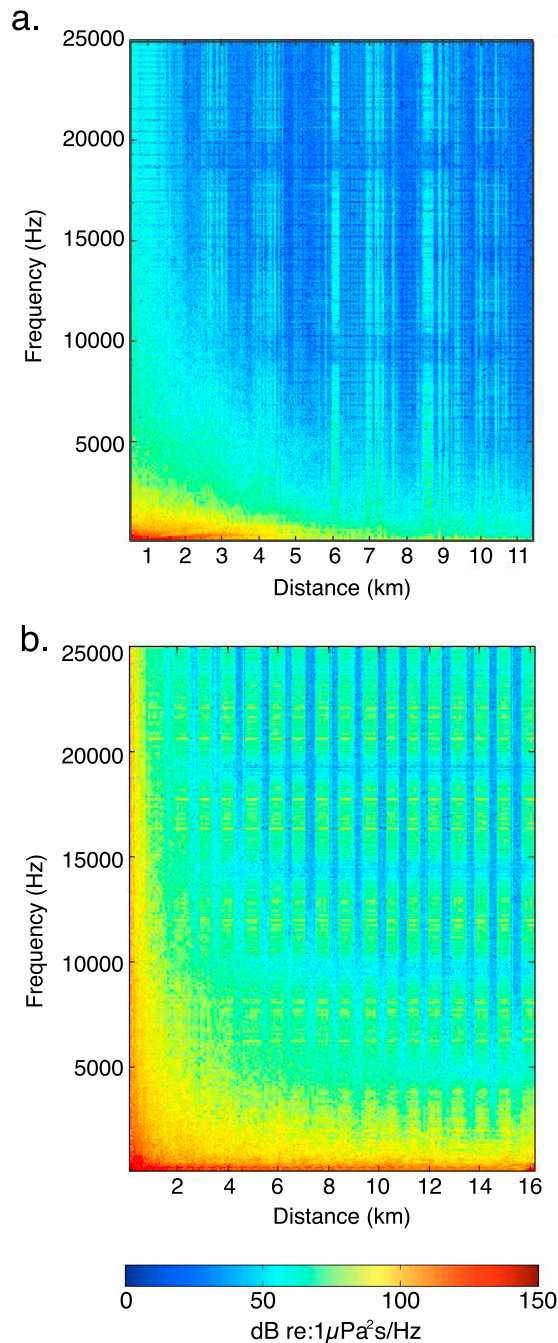


Figure 18. (a) Energy spectral density versus distance for inline shots at the deep site. (b) Energy spectral density versus distance for inline shots at the shallow site. Note the horizontal and vertical lines are due to leakage of a noise burst associated with the GPS receiver on the buoy and are not related to the R/V *Marcus Langseth* sound source. See text for a full discussion. Color scale is the same for both plots.

[43] In shallow water, it has been shown that sound exposure levels determined from arrivals recorded with a towed MCS array match calibration levels very well. Additional work would be needed to predict the entire range of water depths in which this observation is true, but it does suggest that, in some environments, sound exposure levels may be observed on site and in real time, allowing mitigation efforts to be adjusted accordingly.

Acknowledgments

[44] This work was supported by NSF grant OCE-0624599. We thank two anonymous reviewers for constructive comments that improved the manuscript. We thank the captain, crew, and technical and science party of MGL0707 and MGL0802. This paper is LDEO contribution 7414.

References

- Barton, P. J., J. Diebold, and S. Gulick (2006), Water-borne noise levels from airgun arrays—examples from surprisingly quiet Chicxulub survey, paper presented at 68th EAGE Conference and Exhibition, Eur. Assoc. of Geosci. and Eng., Vienna.
- Diebold, J. B., and P. L. Stoffa (1981), The travelttime equation, tau-p mapping and inversion of common midpoint data, *Geophysics*, *46*(3), 238–254, doi:10.1190/1.1441196. (Reprinted in *Slant-Stack Processing, Geophys. Reprint Ser.*, vol. 14, edited by G. H. F. Gardner and F. K. Levin, pp. 151–167, Soc. of Explor. Geophys., Tulsa, Okla., 1991.)
- Diebold, J. B., M. Tolstoy, P. J. Barton, and S. P. Gulick (2006), Propagation of exploration seismic sources in shallow water, *Eos Trans. AGU*, *87*(36), Jt. Assem. Suppl., Abstract OS41A-03.
- Levin, F. K. (1971), Apparent velocity from dipping interface reflections, *Geophysics*, *36*, 510–516, doi:10.1190/1.1440188.
- Madsen, P. T. (2005), Marine mammals and noise: Problems with root mean square sound pressure levels for transients, *J. Acoust. Soc. Am.*, *117*, 3952–3957, doi:10.1121/1.1921508.
- Southall, B. L., et al. (2007), Marine mammal noise exposure criteria: Initial scientific recommendations, *Aquat. Mamm.*, *33*(4), 411–521.
- Tolstoy, M., J. B. Diebold, S. C. Webb, D. R. Bohnenstiehl, E. Chapp, R. C. Holmes, and M. Rawson (2004), Broadband calibration of R/V *Ewing* seismic sources, *Geophys. Res. Lett.*, *31*, L14310, doi:10.1029/2004GL020234.
- Tolstoy, M., J. Diebold, L. Doermann, S. Nooner, S. C. Webb, D. R. Bohnenstiehl, T. J. Crone, and R. C. Holmes (2009), Broadband calibration of the R/V *Marcus G. Langseth* four-string seismic sources, *Geochem. Geophys. Geosyst.*, *10*, Q08011, doi:10.1029/2009GC002451.